INTERNATIONAL JOURNAL FOR NUMERICAL METHODS IN FLUIDS
Int. J. Numer. Meth. Fluids 2006; **50**:987–1001
Published online 31 October 2005 in Wiley InterScience (www.interscience.wiley.com). DOI: 10.1002/fld.1098

Effect of blockage on critical parameters for flow past a circular cylinder

Bhaskar Kumar[‡] and Sanjay Mittal[*,†]

Department of Aerospace Engineering, Indian Institute of Technology Kanpur, UP 208 016, India

SUMMARY

The effect of location of the lateral boundaries, of the computational domain, on the critical parameters for the instability of the flow past a circular cylinder is investigated. Linear stability analysis of the governing equations for incompressible flows is carried out via a stabilized finite element method to predict the primary instability of the wake. The generalized eigenvalue problem resulting from the finite element discretization of the equations is solved using a subspace iteration method to get the most unstable eigenmode. Computations are carried out for a large range of blockage, $0.005 \leqslant D/H \leqslant 0.125$, where D is the diameter of the cylinder and H is the lateral width of the domain. A non-monotonic variation of the critical Re with the blockage is observed. It is found that as the blockage increases, the critical Re for the onset of the instability first decreases and then increases. However, a monotonic increase in the non-dimensional shedding frequency at the onset of instability, with increase in blockage, is observed. The increased blockage damps out the low-frequency modes giving way to higher frequency modes. The blockage is found to play an important role in the scatter in the data for the non-dimensional vortex shedding frequency at the onset of the instability, from various researchers in the past. Copyright © 2005 John Wiley & Sons, Ltd.

KEY WORDS: Hopf bifurcation; circular cylinder; linear stability analysis; finite element method; blockage

1. INTRODUCTION

It is well known that the steady flow past a circular cylinder looses stability beyond $Re \sim 47$. There have been several attempts, both numerical and experimental, to estimate the critical Reynolds number (Re_c) and the non-dimensional vortex shedding frequency (St_c) at Re_c. Table I lists these values reported by various researchers. For numerical studies, the method

*Correspondence to: S. Mittal, Department of Aerospace Engineering, Indian Institute of Technology Kanpur, UP 208 016, India.
†E-mail: smittal@iitk.ac.in
‡E-mail: bhaskar@iitk.ac.in

Received 6 March 2005
Revised 29 August 2005
Accepted 30 August 2005

Table I. Uniform flow past a circular cylinder: summary of the critical parameters at the onset of wake instability, from various studies.

Researcher(s)	Re_c	St_c	Method	Grid points	Domain size $L \times H$
Kovasznay [1]	40		Experiments		$H = 1250D$
Roshko [2]	40	0.12	Experiments		$H = 1250D$
Berger [3]	50	0.12	Experiments		
Coutanceau and Bouard [4]	34–43	—	Experiments		
Williamson [5]	47.9	0.122	Experiments		$H = 150D$
Norberg [6, 7]	47.4 ($\pm$0.5)	0.1177	Experiments		$H = 6250D$
Gresho [8]	50	0.14	FEM	1825	
Jackson [9]	46.184	0.13804	FEM with II		$20D \times 10D$
Zebib [10]	39–43	0.11–0.13	Eigenvalue anal.		
Ding and Kawahara [11]	46.389	0.12619	FEM AR	9870	$36D \times 16D$
Morzynski and Thiele [12]	46.270	0.13451	FDM with NR	3200	
Chen *et al.* [13]	47.9	0.138	FEM with SI		
Morzynski *et al.* [14]	47	0.1320	FEM with SI	15 838	$20D \times 10D$
Present calculation	47.336	0.1168	FEM with SI	34 324	$100D \times 200D$

The abbreviations used in the table are: FEM, finite element method; II, inverse iteration method; FDM, finite difference method; AR, Arnoldi's method; SI, subspace iteration method.

used and domain size are also listed. A relatively large scatter in the data, especially for St_c, is observed.

Another issue, related to vortex shedding, that has received some attention in the past is the effect of the location of lateral boundaries on the critical parameters. Shair *et al.* [15] have pointed out that although the effect of confining walls is of a secondary nature in the study of flow past a solid body, the stability of the wake is drastically affected by them. They observed a very rapid increase in Re_c with increase in blockage, D/H. Here, H is the lateral width of the domain and D is the diameter of the cylinder. Coutanceau and Bouard [4] found that Re_c increases linearly with increase in blockage. They predicted $Re_c \sim 34$ for the unbounded flow. Chen *et al.* [13] carried out calculations for D/H in the range of 0.1–0.7. They reported results from two sets of computations. The first case, for which their results are shown in Table I, corresponds to the simulation of unbounded flow. The second one is the flow past a cylinder confined in a channel. A parabolic velocity profile was specified at the channel inlet while a no-slip condition was imposed on the velocity at the channel walls. For this case, with very narrow channel, they observed a non-monotonic behaviour in the variation of Re_c with blockage. Sahin and Owens [16] confirmed the findings of Chen *et al.* [13] and observed a similar non-monotonic behaviour for high blockage. For $D/H = 0.64$ they reported Re_c and St_c as high as 284.56 and 0.4351, respectively. They also found that, for very high blockage, multiple steady states are possible.

The objective of the present work is to investigate the effect of blockage on the critical parameters at the onset of vortex shedding for modelling the unconfined flow past a cylinder. To this effect we carry out computations for a wide range of blockage ($0.005 \leqslant D/H \leqslant 0.125$). It is found that the blockage affects the critical parameters quite significantly. While the variation of St_c is monotonic with D/H, an interesting, non-monotonic behaviour of Re_c with D/H is observed. The influence of the location of the upstream and downstream boundaries

of the computational domain has also been investigated. It is also useful to point out that the range of blockage being considered in the present work is representative of the various investigations carried out by different researchers in the past to study unbounded flow past a cylinder. This, to our knowledge, is the first time a systematic study of this kind has been undertaken. Some of the earlier studies like the ones by Chen *et al.* [13] and Sahin and Owens [16] are for very high blockage ratios.

A stabilized finite element formulation is used that allows one to employ equal-order-interpolation functions for velocity and pressure. The SUPG (streamline-upwind/Petrov–Galerkin) and PSPG (pressure-stabilizing/Petrov–Galerkin) stabilization technique [17] is employed to stabilize the computations against spurious numerical oscillations. The formulation for the linear stability analysis with the stabilized finite element method, being used here, was proposed in one of our earlier articles [18]. First, the steady-state solutions at various *Re* are obtained by solving the governing equations by dropping the unsteady terms and progressively increasing the *Re*. The linear stability analysis, of these steady states, involves the solution to an eigenvalue problem. A sub-space iteration procedure [14] in conjunction with shift-invert transformation is utilized.

2. THE GOVERNING EQUATIONS

2.1. The incompressible flow equations

Let $\Omega \subset \mathbb{R}^{n_{sd}}$ and $(0, T)$ be the spatial and temporal domains, respectively, where n_{sd} is the number of space dimensions, and let Γ denote the boundary of Ω. The spatial and temporal coordinates are denoted by $\mathbf{x}$ and t. The Navier–Stokes equations governing incompressible fluid flow are

$$\rho\left(\frac{\partial \mathbf{u}}{\partial t} + \mathbf{u}\cdot\nabla\mathbf{u} - \mathbf{f}\right) - \nabla\cdot\boldsymbol{\sigma} = \mathbf{0} \quad \text{on } \Omega\times(0,T) \tag{1}$$

$$\nabla\cdot\mathbf{u} = 0 \quad \text{on } \Omega\times(0,T) \tag{2}$$

Here ρ, $\mathbf{u}$, $\mathbf{f}$ and $\boldsymbol{\sigma}$ are the density, velocity, body force and the stress tensor, respectively. The stress tensor is written as the sum of its isotropic and deviatoric parts:

$$\boldsymbol{\sigma} = -p\mathbf{I} + \mathbf{T}, \quad \mathbf{T} = 2\mu\boldsymbol{\varepsilon}(\mathbf{u}), \quad \boldsymbol{\varepsilon}(\mathbf{u}) = \tfrac{1}{2}\left((\nabla\mathbf{u}) + (\nabla\mathbf{u})^{\mathrm{T}}\right) \tag{3}$$

where p and μ are the pressure and coefficient of dynamic viscosity, respectively.

2.2. Problem set up and boundary conditions

The cylinder resides in a computational domain whose outer boundary is a rectangle. A schematic of the problem set up is shown in Figure 1. The structure of the mesh is same as used in our earlier studies [18]. A typical mesh is shown in Figure 2. For calculating the steady-state flow following boundary conditions are applied. Free-stream value is assigned to the velocity at the upstream boundary. At the downstream boundary, a Neumann-type

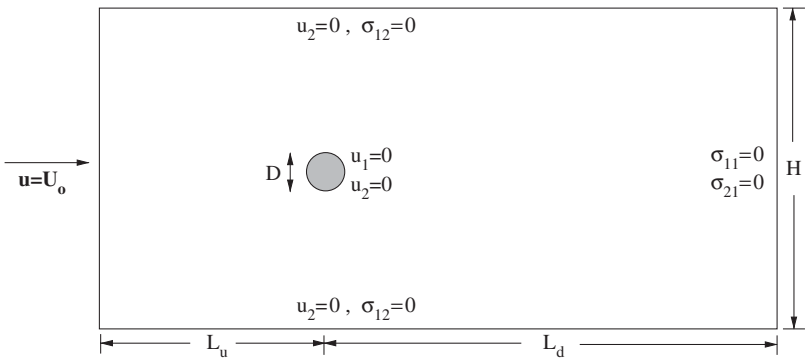

Figure 1. Uniform flow past a cylinder: problem description.

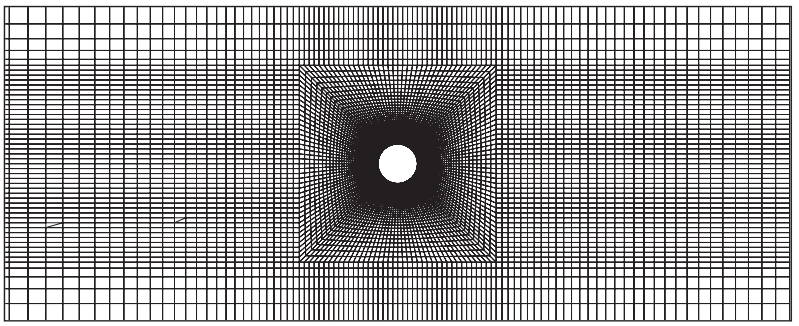

Figure 2. Linear stability analysis of uniform flow past a cylinder: a close-up view of the finite element mesh for $H/D = 8$. The mesh consists of 17 310 nodes and 17 000 quadrilateral elements.

boundary condition for the velocity is specified that corresponds to zero stress vector. On the upper and lower boundaries a 'slip-wall' boundary condition is employed, i.e. the component of velocity normal to and the component of stress vector along these boundaries are prescribed a zero value. For the linear stability analysis, the boundary conditions are the homogeneous versions of the ones used for determining the steady-state solutions.

2.3. Equations for the linear stability analysis of the flow

To conduct a global, linear stability analysis of a non-parallel flow the unsteady solution is expressed as a combination of the steady solution and the disturbance:

$$\mathbf{u} = \mathbf{U} + \mathbf{u}', \quad p = P + p' \tag{4}$$

Here, $\mathbf{U}$ and P represent the steady-state solution whose stability is to be determined while $\mathbf{u}'$ and p' are the perturbation fields of the velocity and pressure, respectively. Substituting Equation (4) in Equations (1)–(2) and subtracting from them, the equations for steady flow,

one obtains:

$$\rho\left(\frac{\partial \mathbf{u}'}{\partial t}+\mathbf{u}'\cdot\nabla\mathbf{U}+\mathbf{U}\cdot\nabla\mathbf{u}'\right)-\nabla\cdot\boldsymbol{\sigma}'=\mathbf{0}\quad\text{on }\Omega\times(0,T)\tag{5}$$

$$\nabla\cdot\mathbf{u}'=0\quad\text{on }\Omega\times(0,T)\tag{6}$$

Here, $\boldsymbol{\sigma}'$ is the stress tensor for the perturbed solution computed using Equation (3). We further assume that the disturbances are small and of the following form:

$$\mathbf{u}'(\mathbf{x},t)=\hat{\mathbf{u}}(\mathbf{x})\mathrm{e}^{\lambda t}\tag{7}$$

$$p'(\mathbf{x},t)=\hat{p}(\mathbf{x})\mathrm{e}^{\lambda t}\tag{8}$$

Substituting Equations (7)–(8) in Equations (5)–(6) we get

$$\rho(\lambda\hat{\mathbf{u}}+\hat{\mathbf{u}}\cdot\nabla\mathbf{U}+\mathbf{U}\cdot\nabla\hat{\mathbf{u}})-\nabla\cdot\hat{\boldsymbol{\sigma}}=\mathbf{0}\quad\text{on }\Omega\tag{9}$$

$$\nabla\cdot\hat{\mathbf{u}}=0\quad\text{on }\Omega\tag{10}$$

Here, λ is the eigenvalue of the fluid system and governs its stability. In general, $\lambda=\lambda_r+i\lambda_i$ where, λ_r and λ_i are the real and imaginary parts, respectively. The boundary conditions for $\hat{\mathbf{u}}$ and $\hat{p}$ are the homogeneous versions of the ones for $\mathbf{U}$ and P as shown in Figure 1.

3. THE FINITE ELEMENT FORMULATION

Consider a finite element discretization of Ω into subdomains Ω^e, $e=1,2,\ldots,n_{el}$, where n_{el} is the number of elements. Based on this discretization, for velocity and pressure perturbation fields we define the finite element trial function spaces $\hat{\mathscr{S}}_{\mathbf{u}}^h$ and $\hat{\mathscr{S}}_p^h$, and weighting function spaces $\hat{\mathscr{V}}_{\mathbf{u}}^h$ and $\hat{\mathscr{V}}_p^h$. These function spaces are selected, by taking the Dirichlet boundary conditions into account, as subsets of $[\mathbf{H}^{1h}(\Omega)]^2$ and $\mathbf{H}^{1h}(\Omega)$, where $\mathbf{H}^{1h}(\Omega)$ is the finite-dimensional function space over Ω. The application of the stabilized finite element method to the perturbation equations, (9) and (10), result in the following formulation: find $\hat{\mathbf{u}}^h\in\hat{\mathscr{S}}_{\mathbf{u}}^h$ and $\hat{p}^h\in\hat{\mathscr{S}}_p^h$ such that $\forall\hat{\mathbf{w}}^h\in\hat{\mathscr{V}}_{\mathbf{u}}^h$ and $\hat{q}^h\in\hat{\mathscr{V}}_p^h$:

$$\begin{aligned}&\int_\Omega\hat{\mathbf{w}}^h\cdot\rho(\lambda\hat{\mathbf{u}}^h+\mathbf{U}^h\cdot\nabla\hat{\mathbf{u}}^h+\hat{\mathbf{u}}^h\cdot\nabla\mathbf{U}^h)\,\mathrm{d}\Omega+\int_\Omega\hat{\boldsymbol{\varepsilon}}(\hat{\mathbf{w}}^h):\hat{\boldsymbol{\sigma}}(\hat{p}^h,\hat{\mathbf{u}}^h)\,\mathrm{d}\Omega\\&+\int_\Omega\hat{q}^h\nabla\cdot\hat{\mathbf{u}}^h\,\mathrm{d}\Omega+\sum_{e=1}^{n_{el}}\int_{\Omega^e}\frac{1}{\rho}(\tau_{\mathrm{SUPG}}\rho\mathbf{U}^h\cdot\nabla\hat{\mathbf{w}}^h+\tau_{\mathrm{PSPG}}\nabla\hat{q}^h)\\&\cdot[\rho(\lambda\hat{\mathbf{u}}^h+\mathbf{U}^h\cdot\nabla\hat{\mathbf{u}}^h+\hat{\mathbf{u}}^h\cdot\nabla\mathbf{U}^h)-\nabla\cdot\hat{\boldsymbol{\sigma}}(\hat{p}^h,\hat{\mathbf{u}}^h)]\,\mathrm{d}\Omega^e\\&+\sum_{e=1}^{n_{el}}\int_{\Omega^e}\tau_{\mathrm{LSIC}}\nabla\cdot\hat{\mathbf{w}}^h\rho\nabla\cdot\hat{\mathbf{u}}^h\,\mathrm{d}\Omega^e=0\end{aligned}\tag{11}$$

In the variational formulation given by Equation (11), the first three terms constitute the Galerkin formulation of the problem. It is well known that the Galerkin formulation is unstable with respect to the advection operator as the cell Reynolds number (based on the local flow velocity and mesh size) becomes large. Also, not all combinations of velocity and pressure interpolations are admissible in the Galerkin formulation. Elements that do not satisfy the Babuska-Brezzi condition lead to oscillatory solutions and, sometimes, no solution at all. To give stability to the basic formulation, a series of element-level integrals are added. The first series of element-level integrals are the SUPG and PSPG stabilization terms added to the variational formulations [17]. The SUPG formulation for convection dominated flows was introduced by Hughes and Brooks [19] and Brooks and Hughes [20]. The Petrov–Galerkin term for Stokes flows, to admit the use of equal-order interpolations for velocity and pressure without producing oscillations in the pressure field, was proposed by Hughes *et al.* [21]. Tezduyar *et al.* [17] proposed a formulation using the SUPG and PSPG stabilizations for finite Reynolds number flows. The second series of element level integrals are stabilization terms based on the least squares of the divergence-free condition on the velocity field. Presently, same definition for τ_{PSPG} and τ_{SUPG} is being used. It is given by the following relation based on its values for the advection and diffusion limits:

$$\tau_{\mathrm{SUPG}} = \tau_{\mathrm{PSPG}} = \left(\frac{1}{\tau_{\mathrm{ADV}}^2} + \frac{1}{\tau_{\mathrm{DIF}}^2} \right)^{-1/2} \tag{12}$$

where

$$\tau_{\mathrm{ADV}} = \frac{h^e}{2\|\mathbf{U}^h\|}, \quad \tau_{\mathrm{DIF}} = \frac{(h^e)^2}{12\nu} \tag{13}$$

Here, h^e is the element length and various definitions have been used by researchers in the past. Mittal [22] conducted a systematic numerical study to investigate the effect of high aspect ratio elements on the performance of the finite element formulation for three commonly used definitions of h^e. In this work we use the definition based on the minimum edge length of an element. The coefficient τ_{LSIC} is defined as

$$\tau_{\mathrm{LSIC}} = \left(\frac{1}{\delta_{\mathrm{ADV}}^2} + \frac{1}{\delta_{\mathrm{DIF}}^2} \right)^{-1/2} \tag{14}$$

where

$$\delta_{\mathrm{ADV}} = \frac{h^e\|\mathbf{U}^h\|}{2}, \quad \delta_{\mathrm{DIF}} = \frac{(h^e)^2(\|\mathbf{U}^h\|)^2}{12\nu} \tag{15}$$

For a description of alternative definitions of the stabilization coefficients the interested reader may refer to the article by Tezduyar [23].

4. THE EIGENVALUE PROBLEM

Equation (11) leads to a generalized eigenvalue problem of the form $\mathbf{A}X - \lambda\mathbf{B}X = 0$, where $\mathbf{A}$ and $\mathbf{B}$ are nonsymmetric matrices. Various algorithms have been developed, in the past, to solve such eigenvalue problems with large sparse nonsymmetric matrices. For example,

some of the methods are the inverse iteration [24], subspace/simultaneous iteration [25] and Lanczos method [26]. In the present case, the situation is complicated by the fact that the continuity equation, which is responsible for determining the pressure, causes the matrix **B** to become singular. Fortunately, in the context of linear stability analysis, we only need to track the leading/rightmost eigenvalue (the eigenvalue with the largest real part). In this study we use the shift-invert transformation in conjunction with the subspace iteration method [27].

The flow past a cylinder is known to undergo a Hopf bifurcation. The steady-state solution loses its stability such that the eigenvalue giving rise to the loss of stability (the rightmost eigenvalue) crosses the imaginary axis with a finite imaginary part. This marks the transition of the stationary flow to a periodic flow. The imaginary part of the unstable eigenvalue gives the angular frequency corresponding to that particular mode. The non-linear terms in the Navier–Stokes equation becomes important as the unstable solution grows. Eventually, the flow achieves a limit-cycle. Therefore, the linear stability analysis can, at best, predict the onset of instability.

5. RESULTS

5.1. *Effect of blockage*

To investigate the effect of blockage, computations with various values of domain size (H/D) are carried out. The location of the upstream and downstream boundaries are each fixed at $50D$, from the centre of the cylinder. The finite element meshes for various H/D are generated so that the spatial resolution is same, as far as possible, in all the cases. We refer to this family of meshes by $R2$. For example, the mesh with $H/D = 100$ consists of 28 170 nodes and 27 800 quadrilateral elements while the one with $H/D = 20$ has 20 206 nodes and 19 880 elements. A close-up view of a typical mesh, for $H/D = 8$ is shown in Figure 2.

Figure 3 shows the variation of the critical parameters with the domain size. A curve fit to the data for various blockage is computed to estimate the Re_c and St_c values for the infinite domain. The curve fits for the data are given as

$$Re_c = 47.3804 - 4.70659/\sqrt{B} + 124.836/B - 1228.84/\sqrt{B^3} + 4334.98/B^2 - 4947/\sqrt{B^5} \quad (16)$$

$$St_c = 0.116311 + 0.0403825B + 1.81145B^2 - 3.97608B^3 \quad (17)$$

where $B = D/H$ is the blockage. It is seen that the values of Re_c and St_c predicted for the infinite domain case are 47.380 and 0.1163, respectively. As the blockage increases, first Re_c decreases and then it increases. Such a non-monotonic variation of Re_c for this range of blockage has not been reported earlier. The vortex shedding frequency, at the onset of the instability, is also found to be quite sensitive to blockage. A monotonic increase in St_c with increase in blockage is observed. Behr *et al.* [28] conducted a numerical investigation for the $Re = 100$ flow past a cylinder to study the sensitivity of flow parameters to H/D. They observed the same trend as in the present study that St_c decreases with increase in H/D. In general, as compared to Re_c, St_c is more sensitive to blockage. For example, for a mesh with $H/D = 9$, compared to the value for infinite domain, $\sim 18.4\%$ higher value of St_c is predicted. On the contrary, the error in Re_c is less than 1%.

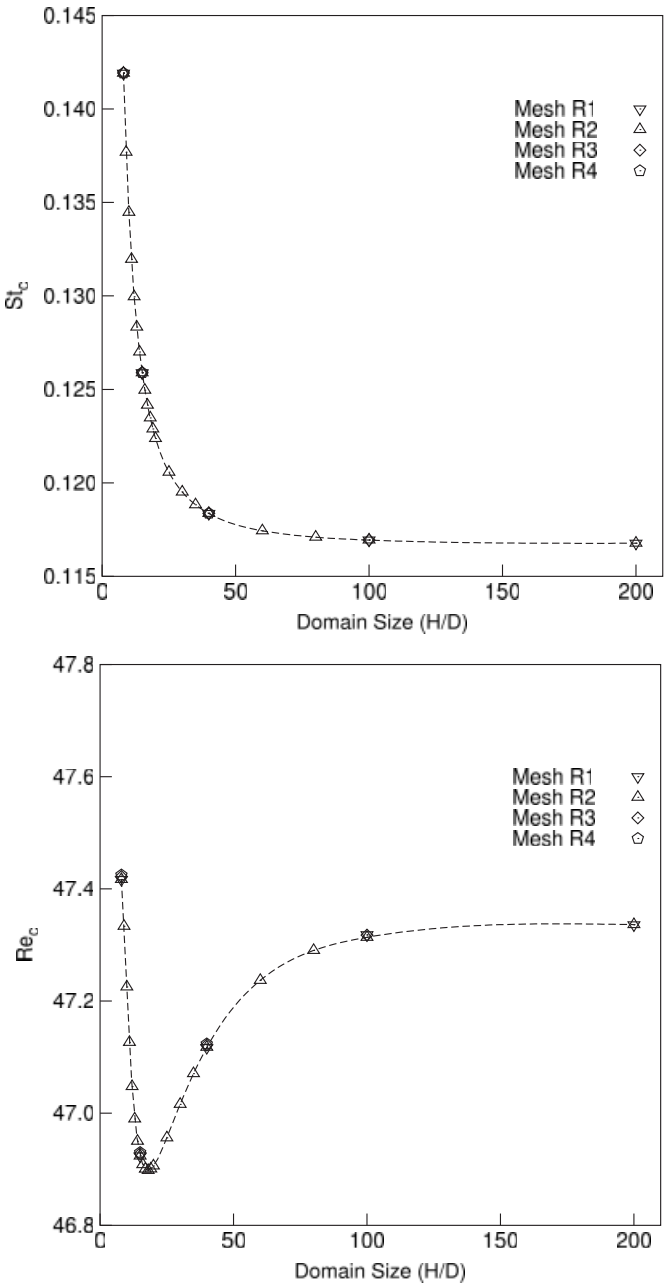

Figure 3. Linear stability analysis of uniform flow past a cylinder with meshes of different spatial resolution: effect of the lateral width of the domain (H/D) on St_c (above) and Re_c (below). In all the cases the upstream and downstream boundaries are located at $50D$, each, from the centre of the cylinder.

5.2. Convergence: adequacy of the spatial resolution

We now investigate the adequacy of the meshes of the family $R2$ in computing these flows. A convergence study with four different families of meshes of increasing spatial resolution, represented by $R1$, $R2$, $R3$ and $R4$, is carried out for different values of H/D. $R1$ represents the family of coarsest meshes while $R4$ is the collection of meshes with maximum resolution. For all the cases, the upstream and downstream boundaries, are each located at $50D$, from the centre of the cylinder. For example, the mesh with $H/D = 40$ belonging to $R1$ family consists of 20 800 quadrilateral elements. The corresponding numbers for the $R2$, $R3$ and $R4$ meshes are 22 400, 25 600 and 30 400, respectively. Figure 3 shows the variation of the critical parameters with the lateral domain size, computed with meshes of various spatial resolution. Excellent agreement is seen between the results from different grids to the extent that the data points are virtually indistinguishable from each other. This, therefore, establishes the adequacy of all the meshes, and in particular the family $R2$, in resolving these flows.

5.3. Effect of upstream and downstream location of the boundaries of computational domain

We would now like to find out if the location of the upstream and downstream boundaries also affect the critical parameters at the onset of the wake instability. To investigate this effect the lateral dimension of the domain is fixed to $H/D = 16$. Computations are carried out for different values of the upstream (L_u) and downstream (L_d) location of the boundaries of the computational domain. The results from the study are shown in Table II. It is observed that while the location of the inlet and outflow boundaries have some effect on Re_c, the St_c is virtually unaffected. Another interesting observation that can be made from Tables I and II is the comparison between the predictions from the work of Ding and Kawahara [11] and the present computations. When we use the same domain size as the one used by Ding and Kawahara [11] ($L \times H = 36D \times 16D$) our results are in excellent agreement with theirs, despite the differences in the two formulations. Overall, it appears that St_c is fairly independent of the streamwise size of the computational domain. On the other hand, the critical Re does show some dependence on the streamwise length of the domain.

A logical question that comes up is: what is the effect of blockage on the critical parameters for truncated streamwise domain sizes? Does Re_c still show a non-monotonic variation with H/D? Different values of the streamwise length of the domain have been employed by different

Table II. Effect of upstream and downstream boundary location on the Re_c and St_c for $H/D = 16$.

L_u	L_d	Re_c	St_c
8	28	46.384	0.126
16	28	46.735	0.125
50	50	46.908	0.125

L_u and L_d indicate the upstream and downstream boundary location respectively from the centre of the cylinder in terms of the diameter of the cylinder.

researchers in the past. For example, the distance of the downstream boundary from the cylinder is $15D$, each, in the computations by Morzynski *et al.* [14] and Jackson [9] while it is $28D$ for the grid used by Ding and Kawahara [11]. To compare our results with those from previous studies we carry out computations with approximately the same domain size as used by others. To this extent, the size of the computational domain is chosen such that for $H/D \leqslant 13$, the upstream and downstream boundaries are located at $10D$, each, from the cylinder. For larger H/D, the streamwise location of the two boundaries is $20D$ and $50D$, respectively. The meshes associated with these domains with smaller streamwise length are collectively referred to as M. The results from the computations are shown in the Figure 4.

The non-monotonic variation of Re_c with H/D and monotonic decrease in St_c with H/D is observed for the all the locations of upstream and downstream boundaries that we have studied. While the effect of the streamwise extent of the domain on St_c is insignificant, it is clear from the computations that, the non-monotonic variation of Re_c with H/D is amplified for shorter streamwise length of the domain. Compared to the larger domain, the minimum value of Re_c decreases from 46.898 to 46.392 and the lateral width, H/D, at which the minimum occurs decreases from 18 to 13. The curve fits for the variation of the critical parameters with the blockage ($B = D/H$) using mesh M are: $Re_c = 47.5548 - 23.5598B + 21.821B^2 + 1175.91B^3$, and $St_c = 0.115784 + 0.102434B + 0.86421B^2$.

5.4. *The scatter of data from various computational investigations*

Listed in Table I are the values reported by various researchers for the critical parameters. A relatively large scatter in the data, especially for St_c for the computational studies, is observed. The computational method used and domain size are also listed. It is seen from Figures 3 and 4 that the critical parameters vary significantly with the blockage. We have seen, earlier in the paper, that the location of the upstream and downstream boundaries have some effect on the Re_c but St_c is largely unaffected. We now attempt to examine the scatter in the data reported by various computational studies in the context of the location of boundaries of the computational domain.

Shown in Figure 4 are the critical parameters for various values of blockage (for two sizes of the domain in the stream-wise direction) along with the results reported by other researchers. The data for St_c from other studies is in excellent agreement with the present results. Therefore, it can be concluded that the scatter in the data for St_c from various studies can be attributed to the blockage effects. The scatter in the Re_c seems to depend on, both, the blockage as well as the streamwise extent of the domain. It is seen from Figure 4 that the results from the present computations for the domain with shorter streamwise length are in fairly good agreement with the data for Re_c from other studies. Of course, the spatial resolution of the computations and the numerical accuracy of the algorithm employed are also important. The results from Jackson [9] have been computed using a finite element method with two sets of meshes. The coarse mesh with 3056 nodes results in $Re_c = 45.403$ and $St_c = 0.13626$ while the values with the mesh with 12 000 nodes are $Re_c = 46.136$ and $St_c = 0.13793$. For practical reasons, they were unable to use grids with significantly finer resolution. The values listed in Table I (and shown in Figure 4) are the estimated converged values based on the accuracy properties of their element types. It is our belief that further increase in spatial resolution will move the results from Jackson [9] closer to our computational curve shown in Figure 4. In

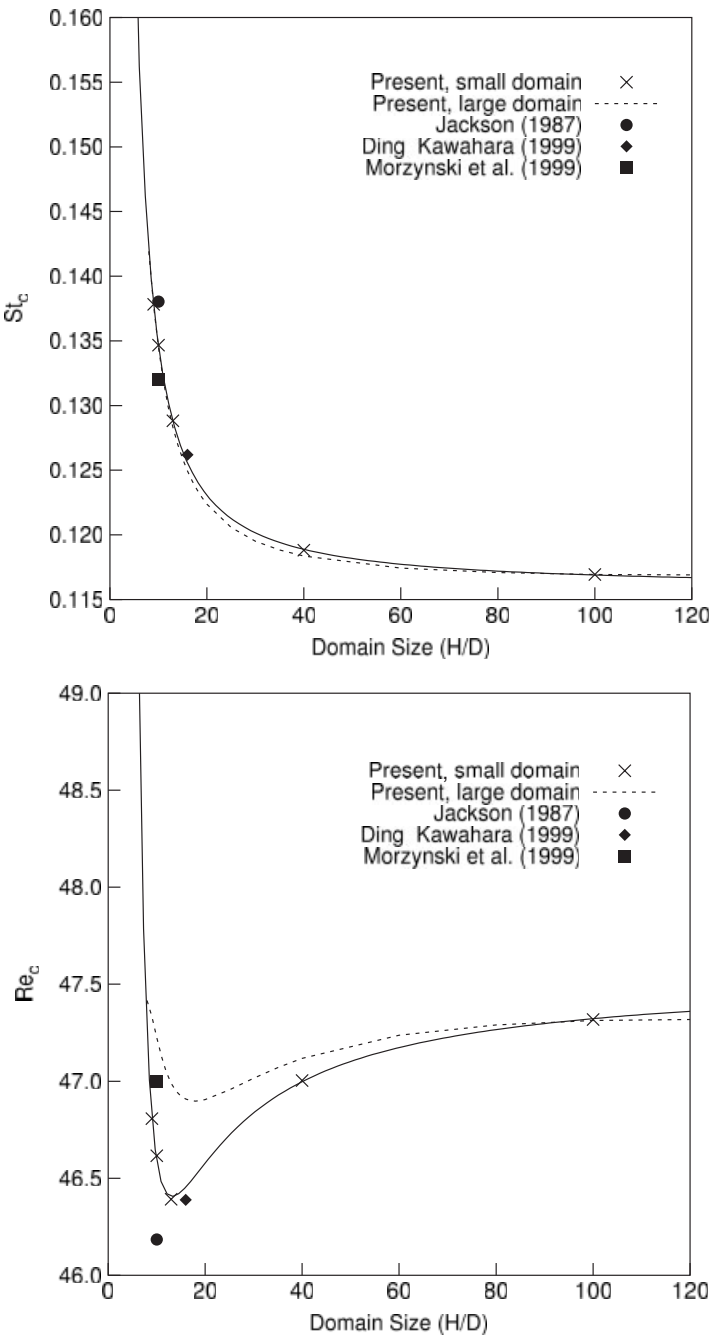

Figure 4. Linear stability analysis of uniform flow past a cylinder: comparison of St_c (above) and Re_c (below) with results from other studies. The results for the large domain are for $L_u = L_d = 50D$. The smaller domain refers to a domain of shorter length in the streamwise direction.

fact, the data from Morzynski *et al.* [14], for the same domain size, agrees quite well with the present computations.

Another important point that can be noted is that because of the non-monotonic variation of Re_c with H/D, it is possible to predict the correct Re_c, for unbounded flow, by choosing an appropriate value of blockage. For example, from the curve fit given above, it is seen that $H/D = 7.6$ results in $Re_c \sim 47.5$. However, such computations overpredict the value of St_c by $\sim 25\%$. For $H/D = 10$, the domain size used by Morzynski *et al.* [14] and Jackson [9], the curve fit predicts $St_c = 0.1347$. This is quite close to the values reported by Morzynski *et al.* [14] and Jackson [9] as shown in Table I. Similarly, for $H/D = 16$, the value predicted by the curve fit, for St_c, is 0.1256 which is again very close to the value reported by Ding and Kawahara [11].

5.5. *The eigenmodes at the onset of instability*

The real and imaginary parts of the unstable eigenmodes of the computed vorticity fields for Re just after the onset of instability are shown in Figure 5. It is clear from the picture that the vorticity field for the steady flow is antisymmetric, about the x-axis, while the perturbations

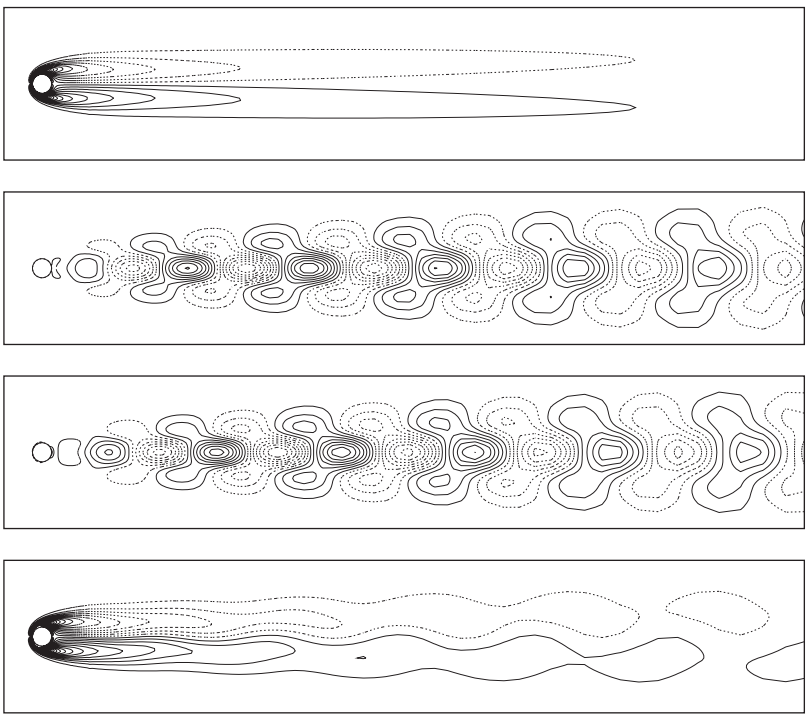

Figure 5. Vorticity field for $Re = 47.4$ flow past a cylinder: (top to bottom) the steady-state solution, real and imaginary parts of the most unstable eigenmode and a linear combination of the steady-state solution and the most unstable eigenmode. The solutions are with $H/D = 100$ and the mesh is from the $R2$ family. The broken lines denote negative while the solid lines represent positive value of the vorticity.

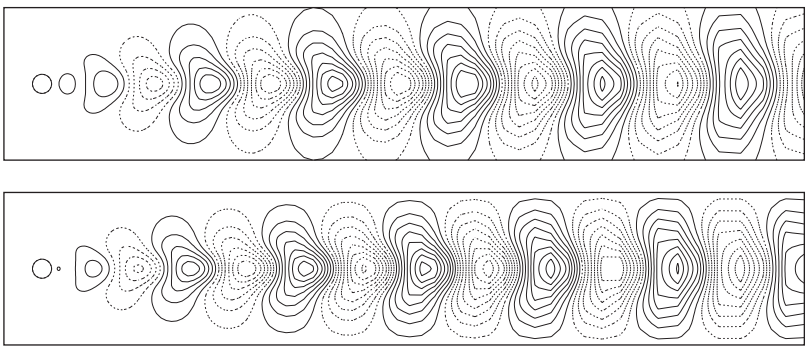

Figure 6. Comparison of the most unstable eigenmodes for the vertical component of velocity at Re_c for meshes with $H/D = 100$ (top) and $H/D = 8$ (bottom) from $R2$ family. The broken lines denote negative while the solid lines represent positive value of the vertical velocity.

are symmetric. These pictures are for $Re = 47.4$ computed with a mesh corresponding to $H/D = 100$ from $R2$ family. They are very similar to the ones from Ding and Kawahara [11]. The appearance of the symmetric perturbations to the antisymmetric base flow and vice versa is the cause of symmetry breaking bifurcation. A combination of the steady flow and the eigenmodes is also shown in Figure 5 to reproduce the asymmetric flow field at the onset of instability.

5.6. A possible explanation of the non-monotonic behaviour of the Re_c with blockage

We propose a possible explanation for the non-monotonic behaviour of the Re_c with blockage. As the blockage increases the local acceleration of the flow near the cylinder causes it to experience a virtually higher Re flow. Therefore, the critical Re, at which the flow becomes unstable, decreases. However, beyond a certain point ($H/D \leqslant 18$ with mesh $R2$), when the blockage is increased further, the boundary condition corresponding to no normal flow across the wall at the lateral boundaries damps the perturbations. This causes the Re_c to increase with blockage. Figure 6 shows the most unstable eigenmodes for the vertical component of velocity at an Re close to the onset of instability computed with two different locations of the lateral boundaries ($H/D = 100$ and 8 from $R2$ family). It can be observed that, for the case with the narrower domain, the lateral boundaries seem to inhibit the growth of the perturbations.

6. CONCLUSIONS

The effect of location of lateral boundaries on estimating the critical parameters for unbounded flow past a circular cylinder have been examined by utilizing a wide range of blockage. A non-monotonic variation of Re_c with blockage is observed and a possible explanation is suggested. The blockage effects are negligible when the lateral boundaries are located more than $100D$ from the cylinder. As the lateral boundaries are brought inwards, the local flow accelerates resulting in a virtually higher Re flow and thereby, lowering the Re_c value. However, further increase in blockage inhibits the growth of perturbations leading to an increase in Re_c. The

non-dimensional vortex shedding frequency at the onset of the instability is found to be very sensitive to the blockage. It increases rapidly with increase in blockage, especially for high blockage. The study is utilized to explain the large scatter in the St_c values reported by various researchers in the past. The Re_c is affected by, both, the lateral as well as the streamwise extent of the domain.

ACKNOWLEDGEMENT

Partial support for this work from the Department of Science and Technology (DTS), India is gratefully acknowledged.

REFERENCES

1. Kovasznay LSG. Hot-wire investigation of the wake behind cylinders at low Reynolds numbers. *Proceedings of the Royal Society*, *Series A* 1949; **198**:174–190.
2. Roshko A. On the development of turbulent wakes from vortex streets. *Technical Report 1191*, NACA, 1954.
3. Berger E, Wille R. Periodic flow phenomena. *Annual Review of Fluid Mechanics* 1972; **4**:313–340.
4. Coutanceau M, Bouard R. Experimental determination of the main features of the viscous flow in the wake of a circular cylinder in uniform translation. Part 1. Steady flow. *Journal of Fluid Mechanics* 1977; **79**:231.
5. Williamson CHK. Oblique and parallel modes of vortex shedding in the wake of a circular cylinder at low Reynolds numbers. *Journal of Fluid Mechanics* 1989; **206**:579–627.
6. Norberg C. An experimental investigation of the flow around a circular cylinder: influence of aspect ratio. *Journal of Fluid Mechanics* 1994; **258**:287–316.
7. Norberg C. Flow around a circular cylinder: aspects of fluctuating lift. *Journal of Fluids and Structures* 2001; **15**:459–469.
8. Gresho PM, Chan ST, Lee TL, Upson CD. A modified finite element method for solving the time-dependent incompressible Navier–Stokes equations. Part 2. Applications. *International Journal for Numerical Methods in Fluids* 1984; **4**:619.
9. Jackson CP. A finite-element study of the onset of vortex shedding in flow past variously shaped bodies. *Journal of Fluid Mechanics* 1987; **182**:23–45.
10. Zebib A. Stability of viscous flow past a circular cylinder. *Journal of Engineering Mathematics* 1987; **21**: 155–165.
11. Ding Y, Kawahara M. Three dimensional linear stability analysis of incompressible viscous flows using the finite element method. *International Journal for Numerical Methods in Fluids* 1999; **31**:451–479.
12. Morzynski M, Thiele F. Numerical stability analysis of a flow about a cylinder. *Zeitschrift fur Angewandte Mathematik und Mechanik* 1991; **71**:T424–T428.
13. Chen JH, Pritchard WH, Tavener SJ. Bifurcation for flow past a cylinder between parallel planes. *Journal of Fluid Mechanics* 1995; **284**:23–41.
14. Morzynski M, Afanasiev K, Thiele F. Solution of the eigenvalue problems resulting from global non-parallel flow stability analysis. *Computer Methods in Applied Mechanics and Engineering* 1999; **169**:161–176.
15. Shair FH, Grove AS, Petersen EE, Archivos A. The effect of confining walls on the stability of the steady wake behind a circular cylinder. *Journal of Fluid Mechanics* 1963; **17**:546–550.
16. Sahin M, Owens RG. A numerical investigation of wall effects up to high blockage ratios on two-dimensional flow past a confined circular cylinder. *Physics of Fluids* 2004; **16**(5):1305–1320.
17. Tezduyar TE, Mittal S, Ray SE, Shih R. Incompressible flow computations with stabilized bilinear and linear equal-order-interpolation velocity-pressure elements. *Computer Methods in Applied Mechanics and Engineering* 1992; **95**:221–242.
18. Mittal S, Kumar B. Flow past a rotating cylinder. *Journal of Fluid Mechanics* 2003; **476**:303–334.
19. Hughes TJR, Brooks AN. A multi-dimensional upwind scheme with no crosswind diffusion. In *Finite Element Methods for Convection Dominated Flows*, Hughes TJR (ed.), AMD-vol. 34. ASME: New York, 1979; 19–35.
20. Brooks AN, Hughes TJR. Streamline upwind/Petrov–Galerkin formulations for convection dominated flows with particular emphasis on the incompressible Navier–Stokes equations. *Computer Methods in Applied Mechanics and Engineering* 1982; **32**:199–259.
21. Hughes TJR, Franca LP, Balestra M. A new finite element formulation for computational fluid dynamics: V. Circumventing the Babuška–Brezzi condition: a stable Petrov–Galerkin formulation of the Stokes problem accommodating equal-order interpolations. *Computer Methods in Applied Mechanics and Engineering* 1986; **59**:85–99.

22. Mittal S. On the performance of high aspect-ratio elements for incompressible flows. *Computer Methods in Applied Mechanics and Engineering* 2000; **188**:269–287.
23. Tezduyar TE. Computation of moving boundaries and interfaces and stabilization parameters. *International Journal for Numerical Methods in Fluids* 2003; **43**:555–575.
24. Wilkinson JH. *The Algebraic Eigenvalue Problem*. Clarendon Press: Oxford, 1965.
25. Stewart GW. Simultaneous iteration for computing invariant subspaces of nonhermitian matrices. *Numerische Mathematik* 1976; **25**:123–136.
26. Meyer A. *Modern Algorithms for Large Sparse Eigenvalue Problems*. Akademie-Verlag: Berlin, 1987.
27. Stewart GW. Methods of simultaneous iteration for calculating eigenvectors of matrices. In *Topics in Numerical Analysis II*, Miller JHH (ed.). Academic Press: New York, 1975; 169–185.
28. Behr M, Hastreiter D, Mittal S, Tezduyar TE. Incompressible flow past a circular cylinder: dependence of the computed flow field on the location of the lateral boundaries. *Computer Methods in Applied Mechanics and Engineering* 1995; **123**:309–316.

